International Journal of Thermal Sciences 49 (2010) 621–630

Contents lists available at ScienceDirect

International Journal of Thermal Sciences

journal homepage: www.elsevier.com/locate/ijts

# Viscous dissipation and thermoconvective instabilities in a horizontal porous channel heated from below

A. Barletta [a,*], L. Storesletten [b]

[a] Dipartimento di Ingegneria Energetica, Nucleare e del Controllo, Ambientale (DIENCA), Università di Bologna, Via dei Colli 16, I–40136 Bologna, Italy
[b] Department of Mathematics, University of Agder, Serviceboks 422, 4604 Kristiansand, Norway

ARTICLE INFO

*Article history:*
Received 3 August 2009
Received in revised form
2 October 2009
Accepted 28 October 2009
Available online 22 November 2009

*Keywords:*
Porous medium
Darcy's law
Viscous dissipation
Linear stability
Convective rolls
Series solution

ABSTRACT

A linear stability analysis of the basic uniform flow in a horizontal porous channel with a rectangular cross section is carried out. The thermal boundary conditions at the impermeable channel walls are: uniform incoming heat flux at the bottom wall, uniform temperature at the top wall, adiabatic lateral walls. Thermoconvective instabilities are caused by the incoming heat flux at the bottom wall and by the internal viscous heating. Linear stability against transverse or longitudinal roll disturbances is investigated either analytically by a power series formulation and numerically by a fourth order Runge-Kutta method. The special cases of a negligible effect of viscous dissipation and of a vanishing incoming heat flux at the bottom wall are discussed. The analysis of these special cases reveals that each possible cause of the convective rolls, bottom heating and viscous heating, can be the unique cause of the instability under appropriate conditions. In all the cases examined, transverse rolls form the preferred mode of instability.



## 1. Introduction

The analysis of the Darcy–Bénard problem in a horizontal fluid saturated porous layer is a classical issue of the studies of stability against thermally-induced convection cells. The importance of the Darcy–Bénard problem and of its several variants stems from the link to the conceptually similar Rayleigh–Bénard problem for a clear fluid. In practice, the interest in the investigation of convective instabilities in a fluid saturated porous material heated from below arises from the several applications either with respect to geophysics, to the hydrology of groundwater, and to the diffusion of chemical contaminants in the soil. A wide literature exists on this subject originated from the pioneering papers by Horton, Rogers [1] and Lapwood [2]. A subsequent extension of this study is Prats problem [3], where a basic horizontal throughflow in the porous layer is assumed, instead of the basic rest state considered in the papers by Horton, Rogers [1] and Lapwood [2]. Comprehensive reviews of this subject, accounting for the wide literature available to date, can be found in Nield and Bejan [4], Rees [5] and Tyvand [6].

Interesting studies about the effect of viscous dissipation on heat transfer and fluid flow in saturated porous media have been published [7–13]. Some of these investigations are devoted to the modelling of the viscous dissipation contribution in the local energy balance [9,12,13]. In particular, Nield [9] discusses the resolution of a paradox arising when both viscous dissipation and inertial effects occur. Breugem and Rees [12] carry out a rigorous volume-averaging procedure for the local balance equations under the assumption of a non negligible viscous dissipation. Several studies have been carried out on the effects of the viscous heating in buoyant flows [7,8,10,11]. For a detailed survey of the wide literature on viscous dissipation in porous media we refer the reader to the book by Nield and Bejan [4], as well as to the recent paper by Nield [13].

Quite recently, the effects of viscous dissipation have been investigated as the possible cause of convective instabilities in porous media [14–19]. In these papers, a fluid saturated porous layer with an infinite horizontal width and a finite thickness is considered. Different flow models and thermal boundary conditions are investigated. Among the cases examined we cite, horizontal basic flow with a bottom adiabatic boundary and a top boundary subject to a third kind condition [14] or with bottom and top adiabatic boundaries [15]. The linear instabilities of the basic horizontal flow of water next to the density maximum state have been studied [16] and the form-drag effects have been included [17]. The Prats problem has been revisited by including both the contributions of viscous dissipation and pressure work in the local energy balance [18]. The case of a basic vertical throughflow with

* Corresponding author. Tel.: +39 51 644 1703; fax: +39 51 644 1747.
*E-mail addresses:* antonio.barletta@unibo.it (A. Barletta), leiv.storesletten@uia.no (L. Storesletten).

1290-0729/$ – see front matter © 2009 Elsevier Masson SAS. All rights reserved.
doi:10.1016/j.ijthermalsci.2009.10.010

**Nomenclature**

| | |
|---|---|
| $a$ | wave number, Eq. (32) |
| $A_n$, $B_n$ | dimensionless coefficients, Eq. (37) |
| $c$ | average heat capacity per unit mass |
| $C_{m,n}$, $D_{m,n}$ | dimensionless coefficients, Eq. (50) |
| $Ec$ | Eckert number, Eq. (9) |
| $\mathbf{g}$ | gravitational acceleration |
| $g$ | modulus of the gravitational acceleration |
| $Ge$ | Gebhart number, Eq. (9) |
| $H$ | channel height |
| $k$ | average thermal conductivity |
| $K$ | permeability |
| $L$ | channel half-width |
| $m$, $n$ | integers |
| $Pe$ | Péclet number, Eq. (19) |
| $\overline{q}_0$ | bottom wall heat flux |
| $Ra$ | Rayleigh number, Eq. (9) |
| $\Re\{\}$, $\Im\{\}$ | real part, imaginary part |
| $s$ | $L/H$, aspect ratio |
| $t$ | dimensionless time, Eq. (9) |
| $T$ | dimensionless temperature, Eq. (9) |
| $\overline{T}_0$ | top wall temperature |
| $u$, $v$, $w$ | dimensionless velocity components, Eq. (9) |
| $U$, $V$, $W$ | dimensionless velocity disturbances, Eq. (20) |
| $x$, $y$, $z$ | dimensionless Cartesian coordinates, Eq. (9) |

*Greek symbols*

| | |
|---|---|
| $\alpha$ | average thermal diffusivity |
| $\beta$ | volumetric coefficient of thermal expansion |
| $\gamma$ | dimensionless coefficient, Eq. (33) |
| $\varepsilon$ | perturbation parameter, Eq. (20) |
| $\eta$, $\eta_m$ | Value of $B_0$, $D_{m,0}$ |
| $\theta$ | dimensionless temperature disturbance, Eq. (20) |
| $\Theta(y)$, $\Theta_m(y)$ | dimensionless functions, Eqs. (32) and (46) |
| $\lambda$ | $\lambda_1 + i\lambda_2$, complex exponential growth rate |
| $\nu$ | kinematic viscosity |
| $\sigma$ | ratio between the volumetric heat capacities of the fluid saturated porous medium and of the fluid |
| $\psi$ | dimensionless streamfunction, Eqs. (28) and (42) |
| $\Psi(y)$, $\Psi_m(y)$ | dimensionless functions, Eqs. (32) and (46) |
| $\Omega$ | dimensionless parameter, Eq. (54) |

*Superscript, subscripts*

| | |
|---|---|
| - | dimensional quantity |
| $B$ | basic flow |
| $cr$ | critical value |
| $L$ | longitudinal rolls |

viscous dissipation has been considered [19], thus extending the analysis carried out by Homsy and Sherwood [20]. All these investigations confirmed that the effect of viscous dissipation may be the sole cause of the convective instabilities. In other words, linear instabilities induced by the effect of viscous dissipation term may arise even in the absence of a heat input across the bottom boundary. These instabilities are in fact thermoconvective instabilities, although generated internally by the viscous heating and not by an externally impressed temperature gradient.

The aim of the present paper is to develop the above described investigation of the role played by the effect of viscous dissipation on the thermoconvective instabilities in porous media. In the present study, the effect of a lateral confinement due to adiabatic vertical boundaries is considered. Reference is made to a porous channel with an isoflux bottom boundary and an isothermal top boundary. The critical conditions for the onset of either transverse or longitudinal rolls are determined both analytically by a power series method and numerically by a fourth order Runge-Kutta method.

## 2. Governing equations

We consider the stability of parallel Darcy flow in a rectangular horizontal channel filled with a fluid saturated porous medium. The channel is bounded above and below by two horizontal walls, separated by a distance $H$, and laterally by two vertical walls separated by a distance $2L$; all walls are impermeable (see Fig. 1). The components of seepage velocity along the $\overline{x}$-, $\overline{y}$- and $\overline{z}$-directions are denoted by $\overline{u}$, $\overline{v}$, and $\overline{w}$ respectively, where the $\overline{y}$-axis is vertical and the $\overline{z}$-axis-axis is directed along the channel. The lower boundary wall $\overline{y} = 0$ is subject to a positive uniform heat flux $\overline{q}_0$, while the upper boundary wall $\overline{y} = H$ is supposed to be isothermal with temperature $\overline{T}_0$. Furthermore, the lateral walls $\overline{x} = \pm L$ are assumed to be adiabatic. Both the Darcy model and the Boussinesq approximation are invoked.

The governing mass, momentum and energy equations can be expressed as

$$\frac{\partial \overline{u}}{\partial \overline{x}} + \frac{\partial \overline{v}}{\partial \overline{y}} + \frac{\partial \overline{w}}{\partial \overline{z}} = 0, \tag{1}$$

$$\frac{\partial \overline{w}}{\partial \overline{y}} - \frac{\partial \overline{v}}{\partial \overline{z}} = -\frac{g\,\beta\,K}{\nu}\frac{\partial \overline{T}}{\partial \overline{z}}, \tag{2}$$

$$\frac{\partial \overline{u}}{\partial \overline{z}} - \frac{\partial \overline{w}}{\partial \overline{x}} = 0, \tag{3}$$

$$\frac{\partial \overline{v}}{\partial \overline{x}} - \frac{\partial \overline{u}}{\partial \overline{y}} = \frac{g\beta K}{\nu}\frac{\partial \overline{T}}{\partial \overline{x}}, \tag{4}$$

$$\sigma\frac{\partial \overline{T}}{\partial \overline{t}} + \overline{u}\frac{\partial \overline{T}}{\partial \overline{x}} + \overline{v}\frac{\partial \overline{T}}{\partial \overline{y}} + \overline{w}\frac{\partial \overline{T}}{\partial \overline{z}} = \alpha\left(\frac{\partial^2 \overline{T}}{\partial \overline{x}^2} + \frac{\partial^2 \overline{T}}{\partial \overline{y}^2} + \frac{\partial^2 \overline{T}}{\partial \overline{z}^2}\right) + \frac{\nu}{Kc}\left(\overline{u}^2 + \overline{v}^2 + \overline{w}^2\right). \tag{5}$$

Eqs. (2)–(4) have been obtained by applying the curl operator to both sides of Darcy's law in order to remove the explicit dependence on the pressure field. In Eq. (5), the dissipation function is proportional to the square modulus of the seepage velocity [13].

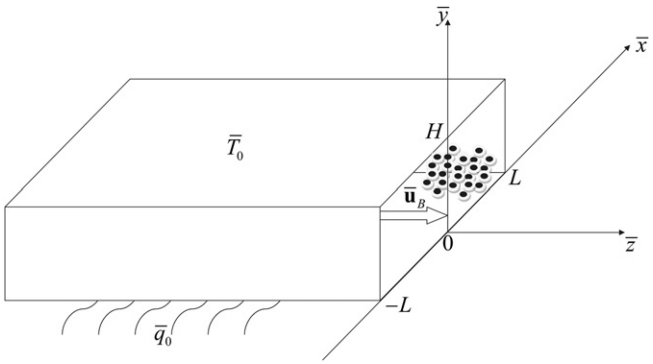


**Fig. 1.** Drawing of the porous channel.

The velocity and temperature conditions at the boundaries are

$$\overline{v} = 0, \quad -k\frac{\partial \overline{T}}{\partial \overline{y}} = \overline{q}_0 \quad \text{on } \overline{y} = 0, \ -L < \overline{x} < L, \tag{6}$$

$$\overline{v} = 0, \quad \overline{T} = \overline{T}_0 \quad \text{on } \overline{y} = H, \ -L < \overline{x} < L, \tag{7}$$

$$\overline{u} = 0, \quad \frac{\partial \overline{T}}{\partial \overline{x}} = 0 \quad \text{on } \overline{x} = \pm L, \ 0 < \overline{y} < H. \tag{8}$$

As described in the following sections, a forced basic flow caused by a horizontal pressure gradient is prescribed within the porous channel. This flow results in a uniform basic velocity profile, with a seepage velocity of magnitude $\overline{w}_B$ in the $\overline{z}$-direction, and a purely vertical heat flux.

### 2.1. Dimensionless formulation

We introduce the following dimensionless quantities:

$$(\overline{x}, \overline{y}, \overline{z}) = (x, y, z)H, \quad \overline{t} = t\frac{\sigma H^2}{\alpha}, \quad (\overline{u}, \overline{v}, \overline{w}) = (u, v, w)\frac{\alpha}{H},$$
$$\overline{T} = \overline{T}_0 + \frac{\overline{q}_0 H}{k}T, \quad Ra = \frac{g\beta K \overline{q}_0 H^2}{k\alpha\nu}, \quad Ge = \frac{g\beta H}{c},$$
$$Ec = \frac{Ge}{Ra} = \frac{k\alpha\nu}{Kc\,\overline{q}_0 H}, \tag{9}$$

where *Ra*, *Ge* and *Ec* are the Darcy–Rayleigh number, Gebhart number and Darcy–Eckert number, respectively.

By employing the dimensionless quantities, Eqs. (1)–(8) can be written as follows:

$$\frac{\partial u}{\partial x} + \frac{\partial v}{\partial y} + \frac{\partial w}{\partial z} = 0, \tag{10}$$

$$\frac{\partial w}{\partial y} - \frac{\partial v}{\partial z} = -Ra\frac{\partial T}{\partial z}, \tag{11}$$

$$\frac{\partial u}{\partial z} - \frac{\partial w}{\partial x} = 0, \tag{12}$$

$$\frac{\partial v}{\partial x} - \frac{\partial u}{\partial y} = Ra\frac{\partial T}{\partial x}, \tag{13}$$

$$\frac{\partial T}{\partial t} + u\frac{\partial T}{\partial x} + v\frac{\partial T}{\partial y} + w\frac{\partial T}{\partial z} = \frac{\partial^2 T}{\partial x^2} + \frac{\partial^2 T}{\partial y^2} + \frac{\partial^2 T}{\partial z^2} + Ec(u^2 + v^2 + w^2), \tag{14}$$

$$v = 0, \quad \frac{\partial T}{\partial y} = -1 \quad \text{on } y = 0, \ -s < x < s, \tag{15}$$

$$v = 0, \quad T = 0, \quad \text{on } y = 1, \ -s < x < s, \tag{16}$$

$$u = 0, \quad \frac{\partial T}{\partial x} = 0 \quad \text{on } x = \pm s, \ 0 < y < 1, \tag{17}$$

where $s = L/H$.

### 2.2. Basic solution

Under the above described conditions there exists a stationary flow with uniform horizontal seepage velocity $\mathbf{u}_B = (u_B, v_B, w_B)$, and a purely vertical heat flux. The basic state, which we shall analyse for stability, is given by

$$u_B = 0, \ v_B = 0, \ w_B = Pe, \ T_B = 1 - y + \frac{1}{2}EcPe^2(1 - y^2), \tag{18}$$

where *Pe* is the Péclet number defined by

$$Pe = \frac{\overline{w}_B H}{\alpha}, \tag{19}$$

and $\overline{w}_B$ is the dimensional basic seepage velocity component in the $\overline{z}$-direction. Obviously, it is not restrictive to assume that $\overline{w}_B > 0$, *i.e.* $Pe > 0$.

### 2.3. Linearisation

Perturbations of the basic state given by Eq. (18) are given as

$$u = u_B + \varepsilon U, \ v = v_B + \varepsilon V, \ w = w_B + \varepsilon W, \ T = T_B + \varepsilon\theta, \tag{20}$$

where $\varepsilon$ is a very small perturbation parameter. On substituting Eq. (20) in Eqs. (10)–(17) and neglecting nonlinear terms of order $\varepsilon^2$, we obtain the linearised stability equations,

$$\frac{\partial U}{\partial x} + \frac{\partial V}{\partial y} + \frac{\partial W}{\partial z} = 0, \tag{21}$$

$$\frac{\partial W}{\partial y} - \frac{\partial V}{\partial z} = -Ra\frac{\partial \theta}{\partial z}, \tag{22}$$

$$\frac{\partial U}{\partial z} - \frac{\partial W}{\partial x} = 0, \tag{23}$$

$$\frac{\partial V}{\partial x} - \frac{\partial U}{\partial y} = Ra\frac{\partial \theta}{\partial x}, \tag{24}$$

$$\frac{\partial \theta}{\partial t} + Pe\frac{\partial \theta}{\partial z} - (EcPe^2 y + 1)V = \frac{\partial^2 \theta}{\partial x^2} + \frac{\partial^2 \theta}{\partial y^2} + \frac{\partial^2 \theta}{\partial z^2} + 2EcPeW, \tag{25}$$

$$\begin{aligned} &V = 0, \quad \frac{\partial \theta}{\partial y} = 0 \quad \text{on} \quad y = 0, \quad -s < x < s, \\ &V = 0, \quad \theta = 0 \quad \text{on} \quad y = 1, \quad -s < x < s, \\ &U = 0, \quad \frac{\partial \theta}{\partial x} = 0 \quad \text{on} \quad x = \pm s, \quad 0 < y < 1, \end{aligned} \tag{26}$$

where Eq. (18) is employed. The linearity of Eqs. (21)–(26) implies that, due to the superposition property, one may treat rolls of different orientations separately with regard to instability. An advantage is that each of these cases can be dealt with by using a purely 2D treatment.

## 3. Instability with respect to rolls

Solutions of the disturbance equations (21)–(26) are sought in the form of periodic rolls. Due to the lateral boundaries, only two kinds of convection rolls can exist: rolls parallel to the *z*-axis, hereafter referred to as longitudinal rolls, and rolls orthogonal to the *z*-axis, hereafter referred to as transverse rolls.

### 3.1. Transverse rolls

Let us first examine transverse rolls, *i.e.* horizontal rolls with axes along the *x*-direction. Then, the analysis of the linear disturbances become two-dimensional with

$$U = 0, \ V = V(y, z, t), \ W = W(y, z, t), \ \theta = \theta(y, z, t). \tag{27}$$

On introducing a streamfunction, $\psi$, such that

$$W=\frac{\partial\psi}{\partial y},\quad V=-\frac{\partial\psi}{\partial z}, \tag{28}$$

then Eqs. (21), (23), and (24) are satisfied identically, while Eqs. (22) and (25) can be rewritten in the form

$$\frac{\partial^2\psi}{\partial y^2}+\frac{\partial^2\psi}{\partial z^2}+Ra\frac{\partial\theta}{\partial z}=0, \tag{29}$$

$$\frac{\partial\theta}{\partial t}+Pe\frac{\partial\theta}{\partial z}+\left(EcPe^2y+1\right)\frac{\partial\psi}{\partial z}=\frac{\partial^2\theta}{\partial y^2}+\frac{\partial^2\theta}{\partial z^2}+2EcPe\frac{\partial\psi}{\partial y}. \tag{30}$$

The corresponding boundary conditions are deduced from Eq. (26), namely

$$\begin{aligned}&\frac{\partial\psi}{\partial z}=0,\quad \frac{\partial\theta}{\partial y}=0\quad\text{on}\quad y=0,\quad -s<x<s,\\ &\frac{\partial\psi}{\partial z}=0,\quad \theta=0\quad\text{on}\quad y=1,\quad -s<x<s.\end{aligned} \tag{31}$$

Solutions of Eqs. (29)–(31) are sought in the form of plane waves,

$$\psi(y,z,t)=\Re\left\{i\Psi(y)e^{\lambda t}e^{iaz}\right\},\quad \theta(y,z,t)=\Re\left\{\Theta(y)e^{\lambda t}e^{iaz}\right\}, \tag{32}$$

where the positive real constant $a$ is the wave number, while $\lambda=\lambda_1+i\lambda_2$ is a complex exponential growth rate to be determined. We set $\lambda_1=0$ in order to investigate neutral stability. Moreover, for numerical convenience we shall also set,

$$\gamma=\lambda_2+aPe. \tag{33}$$

By substituting Eq. (32) in Eqs. (29) and (30), we obtain

$$\Psi''-a^2\Psi+aRa\Theta=0, \tag{34}$$

$$\Theta''-\left(i\gamma+a^2\right)\Theta+2iEcPe\Psi'+a\left(EcPe^2y+1\right)\Psi=0, \tag{35}$$

where the primes denote differentiation with respect to $y$.

The boundary conditions for $\Psi$ and $\Theta$ are easily deduced from Eqs. (31) and (32), namely

$$\begin{aligned}&\Psi=0,\quad \Theta'=0\quad\text{on}\quad y=0,\\ &\Psi=0,\quad \Theta=0\quad\text{on}\quad y=1.\end{aligned} \tag{36}$$

The present stability analysis is based on the ordinary differential equations (34) and (35), subject to the boundary conditions (36).

### 3.1.1. Series solution

Eqs. (34)–(36) can be solved through a power series method by expressing

$$\Psi(y)=\sum_{n=0}^{\infty}\frac{A_n}{n!}y^n,\quad \Theta(y)=\sum_{n=0}^{\infty}\frac{B_n}{n!}y^n. \tag{37}$$

The homogeneity of Eqs. (34)–(36) implies that $\Psi(y)$ is defined only up to an arbitrary overall scale factor, which means that we may set $\Psi'(0)=1$ as a normalization condition. The three known (complex) initial conditions are then

$$A_0=\Psi(0)=0,\quad A_1=\Psi'(0)=1,\quad B_1=\Theta'(0)=0, \tag{38}$$

while $B_0=\Theta(0)=\eta$ will need to be obtained by using the boundary conditions at $y=1$, Eq. (36). Higher order coefficients $A_n$ and $B_n$ may be determined by substituting Eq. (37) into Eqs. (34) and (35) and collecting like powers of $y$. We thus obtain

$$A_2=-aRa\eta,\quad B_2=\left(i\gamma+a^2\right)\eta-2iEcPe, \tag{39}$$

and the recurrence relations

$$\begin{aligned}&A_{n+2}=a^2A_n-aRaB_n,\\ &B_{n+2}=\left(i\gamma+a^2\right)B_n-2iEcPeA_{n+1}\\ &\qquad -aA_n-aEcPe^2nA_{n-1},\ n=1,2,3,\ldots\end{aligned} \tag{40}$$

### 3.2. Longitudinal rolls

Longitudinal rolls, with axes parallel to the $z$-direction, are directed along the rectangular channel. The linear disturbances become two-dimensional in this case as well, with

$$U=U(x,y,t),\quad V=V(x,y,t),\quad W=0,\quad \theta=\theta(x,y,t) \tag{41}$$

On introducing a streamfunction, $\psi$, such that

$$U=\frac{\partial\psi}{\partial y},\quad V=-\frac{\partial\psi}{\partial x}, \tag{42}$$

then Eqs. (21)–(23) are satisfied identically, while Eqs. (24) and (25) can be written in the form

$$\frac{\partial^2\psi}{\partial x^2}+\frac{\partial^2\psi}{\partial y^2}+Ra\frac{\partial\theta}{\partial x}=0, \tag{43}$$

$$\frac{\partial\theta}{\partial t}+\left(EcPe^2y+1\right)\frac{\partial\psi}{\partial x}=\frac{\partial^2\theta}{\partial x^2}+\frac{\partial^2\theta}{\partial y^2}. \tag{44}$$

The corresponding boundary conditions deduced from Eq. (26) are

$$\begin{aligned}&\psi=0,\quad \frac{\partial\theta}{\partial y}=0\quad\text{on}\quad y=0,\quad -s<x<s,\\ &\psi=0,\quad \theta=0\quad\text{on}\quad y=1,\quad -s<x<s,\\ &\psi=0,\quad \frac{\partial\theta}{\partial x}=0\quad\text{on}\quad x=\pm s,\quad 0<y<1.\end{aligned} \tag{45}$$

Steady solutions of Eqs. (43)–(45), corresponding to neutral stability, have the following form:

$$\begin{aligned}&\psi(x,y)=\Psi_m(y)\sin\left[\frac{m\pi}{2}\left(\frac{x}{s}+1\right)\right],\\ &\theta(x,y)=-\Theta_m(y)\cos\left[\frac{m\pi}{2}\left(\frac{x}{s}+1\right)\right],\quad m=1,2,3,\ldots\end{aligned} \tag{46}$$

Eq. (46) substituted into Eqs. (43)–(45) yields the ordinary differential equations

$$\Psi_m''-\left(\frac{m\pi}{2s}\right)^2\Psi_m+\frac{m\pi}{2s}Ra\Theta_m=0, \tag{47}$$

$$\Theta_m''-\left(\frac{m\pi}{2s}\right)^2\Theta_m+\frac{m\pi}{2s}\left(EcPe^2y+1\right)\Psi_m=0,\quad m=1,2,3,\ldots, \tag{48}$$

subject to the boundary conditions

$$\psi_m(0)=\psi_m(1)=0,\quad \Theta_m'(0)=\Theta_m(1)=0. \tag{49}$$

### 3.2.1. Series solutions

Eqs. (47) and (48) subject to the boundary conditions (49) can be solved by a power series method expressing

$$\Psi_m(y)=\sum_{n=0}^{\infty}\frac{C_{m,n}}{n!}y^n,\quad \Theta_m(y)=\sum_{n=0}^{\infty}\frac{D_{m,n}}{n!}y^n. \tag{50}$$

The homogeneity of Eqs. (47)–(49) implies that $\Psi_m$ and $\Theta_m$ are defined only up to an arbitrary overall scale factor, which means that we may set $\Psi'_m(0)=1$. The three known initial conditions are then

$$C_{m,0}=\Psi_m(0)=0,\quad C_{m,1}=\Psi'_m(0)=1,\quad D_{m,1}=\Theta'_m(0)=0, \tag{51}$$

while $D_{m,0}=\Theta_m(0)=\eta_m$ will need to be obtained by using the boundary conditions at $y=1$, Eq. (49). Higher order coefficients $C_{m,n}$ and $D_{m,n}$ may be determined by substituting Eq. (50) into Eqs. (47) and (48) and collecting like powers of $y$. We thus obtain

$$C_{m,2}=-\frac{m\pi}{2s}Ra\eta_m,\quad D_{m,2}=\left(\frac{m\pi}{2s}\right)^2\eta_m, \tag{52}$$

and the recurrence relations

$$C_{m,n+2}=\left(\frac{m\pi}{2s}\right)^2 C_{m,n}-\frac{m\pi}{2s}RaD_{m,n},$$
$$D_{m,n+2}=\left(\frac{m\pi}{2s}\right)^2 D_{m,n}-\frac{m\pi}{2s}\left(C_{m,n}+EcPe^2nC_{m,n-1}\right),\quad n=1,2,3,\ldots \tag{53}$$

## 4. Discussion of the results

### 4.1. Transverse rolls

In addition to the series solution discussed in Section 3.1.1, Eqs. (34)–(36) can be solved numerically by adopting an explicit Runge-Kutta method. The numerical procedure can be easily set up by using the software package *Mathematica* 7.0 (© Wolfram, Inc.). The explicit Runge-Kutta method is available through the built-in function *NDSolve* setting the *Method* option to ExplicitRungeKutta. Eqs. (34)–(36) are solved as an eigenvalue problem for assigned values of $a$, $Pe$ and of the parameter

$$\Omega=GePe^2. \tag{54}$$

The reason for using $\Omega$ instead of $Ge$ as an input parameter is the existence of a special regime where $\Omega\sim O(1)$ and $Pe\to\infty$. This regime is such that the eigenvalue problem for transverse rolls can be made self-adjoint. A detailed analysis of this case can be found in the following Section 4.1.1. We note that the parameter $\Omega$ is used as the governing parameter for the study of linear stability in Barletta et al. [14].

For convenience, Eqs. (34) and (35) are rewritten as

$$\Psi''-a^2\Psi+aRa\Theta=0, \tag{55}$$

$$\Theta''-(i\gamma+a^2)\Theta+\frac{2i\Omega}{PeRa}\Psi'+a\left(\frac{\Omega}{Ra}y+1\right)\Psi=0, \tag{56}$$

where the relationship $Ec=Ge/Ra$, Eq. (9), has been used. These equations are solved with the initial conditions

$$\Psi(0)=0,\quad \Psi'(0)=1,\quad \Theta(0)=\eta_1+i\eta_2,\quad \Theta'(0)=0, \tag{57}$$

discussed in Section 3.1.1. Here, $\eta_1$ and $\eta_2$ are the real part and the imaginary part of $\eta$. The real eigenvalues $Ra$, $\gamma$, $\eta_1$ and $\eta_2$ are determined by solving numerically the complex constraint equations

$$\Psi(1)=0,\quad \Theta(1)=0. \tag{58}$$

This is achieved in *Mathematica* 7.0 by means of the built-in function *FindRoot*. As $a$ is prescribed, the eigenvalue $Ra$ is a function of $a$, $Ra(a)$. On minimizing this function, one determines the critical values $a_{cr}$, $Ra_{cr}$ and $\gamma_{cr}$ for any assigned pair $(\Omega, Pe)$.

We point out that the four real unknowns $\eta_1$, $\eta_2$, $Ra$ and $\gamma$ are not uniquely determined by solving the four real algebraic equations $\Re\{\Psi(1)\}=0$, $\Im\{\Psi(1)\}=0$, $\Re\{\Theta(1)\}=0$ and $\Im\{\Theta(1)\}=0$ for assigned $a$, $\Omega$, $Pe$. In fact, there are infinite neutral stability curves that may exist in the parametric space $(a, Ra)$ for a given pair $(\Omega, Pe)$, corresponding either to the lowest mode of instability or to the higher modes. This is a well known feature of the linear analyses of thermoconvective instability examined in several surveys on this subject (see for instance Nield and Bejan [4], Chapter 6). In the present discussion, the higher modes of instability are not studied as our aim is determining the critical conditions for the onset of convective rolls. This objective is achieved just by considering the lowest neutral stability mode.

A comparison between the series solution discussed in Section 3.1.1, truncated to the first $N$ terms, and the explicit Runge-Kutta solution is displayed in Table 1. These data refer to the neutral stability functions $Ra(a)$ and $\gamma(a)$ for $\Omega=40$ and $Pe=10$. Three sample wave numbers $a=1$, $a=2$ and $a=3$ are considered. Table 1 shows that, with increasing $N$, the series solution results rapidly converge to the Runge-Kutta method results. The agreement is perfect even with $N=25$.

We mention that special limiting cases of Eqs. (55) and (56) can be defined.

#### 4.1.1. Limit $Pe\to\infty$

By assuming $\Omega\sim O(1)$ and $Ra\sim O(1)$, Eqs. (55) and (56) can be easily simplified in the limit $Pe\to\infty$. Since $\Omega$ is kept finite, this limit is in fact a double limit: $Pe\to\infty$ and $Ge\to 0$. The only explicitly imaginary contribution is the $i\gamma$ term in Eq. (56), so that one can solve the eigenvalue problem by setting $\gamma=0$ and $\eta_2=0$. Then, the eigenvalue problem becomes self-adjoint and Eqs. (55)–(57) can be expressed as

$$\Psi''-a^2\Psi+aRa\Theta=0, \tag{59}$$

$$\Theta''-a^2\Theta+a\left(\frac{\Omega}{Ra}y+1\right)\Psi=0, \tag{60}$$

$$\Psi(0)=0,\quad \Psi'(0)=1,\quad \Theta(0)=\eta_1,\quad \Theta'(0)=0, \tag{61}$$

where, since the problem is self-adjoint, the eigenfunctions $\Psi$ and $\Theta$ are now real-valued.

#### 4.1.2. Limit $\Omega\to 0$

Another limiting case is obtained by assuming $Pe\sim O(1)$, $Ra\sim O(1)$ and letting $\Omega\to 0$. This limit has a direct physical significance as it corresponds to $Ge\to 0$, *i.e.* to a negligible effect of viscous dissipation. In this limit, Eqs. (55)–(57) yield

**Table 1**
Transverse rolls: neutral stability values of $Ra$ and $\gamma$ with $\Omega=40$ and $Pe=10$. Comparison between the series solution and the Runge-Kutta solution.

| Method | $a=1$ | | $a=2$ | | $a=3$ | |
|---|---|---|---|---|---|---|
| | $Ra$ | $\gamma$ | $Ra$ | $\gamma$ | $Ra$ | $\gamma$ |
| Series, $N=10$ | 30.634985 | 0.703004 | 10.497103 | 0.804620 | 11.383059 | −0.754542 |
| Series, $N=15$ | 30.550923 | 0.711722 | 10.071665 | 0.981118 | 10.635659 | 0.861900 |
| Series, $N=20$ | 30.550835 | 0.711732 | 10.070433 | 0.982201 | 10.655979 | 0.878759 |
| Series, $N=25$ | 30.550835 | 0.711732 | 10.070433 | 0.982203 | 10.656137 | 0.878788 |
| Series, $N=30$ | 30.550835 | 0.711732 | 10.070433 | 0.982203 | 10.656137 | 0.878788 |
| Runge-Kutta | 30.550835 | 0.711732 | 10.070433 | 0.982203 | 10.656137 | 0.878788 |

$$\Psi'' - a^2\Psi + aRa\Theta = 0, \tag{62}$$

$$\Theta'' - a^2\Theta + a\Psi = 0, \tag{63}$$

$$\Psi(0) = 0, \quad \Psi'(0) = 1, \quad \Theta(0) = \eta_1, \quad \Theta'(0) = 0. \tag{64}$$

Again the problem is made self-adjoint by setting $\gamma = 0$ and $\eta_2 = 0$. The critical values $a_{cr}$, $Ra_{cr}$ are independent of any other parameter and are given by

$$a_{cr} = 2.326215, \quad Ra_{cr} = 27.097628. \tag{65}$$

These are the critical values obtained for the Darcy–Bénard problem without viscous dissipation, for bottom impermeable isoflux boundary and top impermeable isothermal boundary, discussed in Rees [5].

#### 4.1.3. Limit $Ra \to 0$

By taking $Ra \to 0$ with $\Omega \sim O(1)$ and $Pe \sim O(1)$, one considers the very special case of an adiabatic bottom boundary ($\overline{q}_0 \to 0$). This case has been diffusely studied in Barletta et al. [14]. The limit $Ra \to 0$ can be taken in Eqs. (55) and (57) after the rescaling:

$$Ra\Theta \to \Theta, \quad Ra\eta \to \eta. \tag{66}$$

Then, one obtains

$$\Psi'' - a^2\Psi + a\Theta = 0, \tag{67}$$

$$\Theta'' - \left(i\gamma + a^2\right)\Theta + \frac{2i\Omega}{Pe}\Psi' + a\Omega y\Psi = 0, \tag{68}$$

$$\Psi(0) = 0, \ \Psi'(0) = 1, \ \Theta(0) = \eta_1 + i\eta_2, \ \Theta'(0) = 0. \tag{69}$$

In this case, the problem is not self-adjoint. Moreover, it must be formulated in a special way as the eigenvalue $Ra$ has disappeared. In fact, one prescribes $a$ and $Pe$ and determines the eigenvalues $\Omega$, $\gamma$, $\eta_1$ and $\eta_2$ by solving the constraint conditions Eq. (58). One may note that Eqs. (67)–(69) yield a self-adjoint problem when $Pe \to \infty$. Then, in this limit, one has $\gamma = 0$, $\eta_2 = 0$ and the critical values of $a$ and $\Omega$ are given by

$$a_{cr} = 2.44827, \quad \Omega_{cr} = 61.8666. \tag{70}$$

These results are in perfect agreement with those reported in Barletta et al. [14].

#### 4.1.4. Critical values

Tables 2 and 3 include the critical values of $a$, $Ra$ and $\gamma$ obtained for different pairs $(\Omega, Pe)$. The values in the column $Pe \to \infty$ in Table 2 are obtained by solving the self-adjoint eigenvalue problem Eqs. (59)–(61). The values in the line $\Omega \to 0$ in Tables 2 and 3 are obtained by solving the self-adjoint eigenvalue problem Eqs. (62)–(64). These results are independent of $Pe$ as we have pointed out in Section 4.1.2. The data reported in Tables 2 and 3 justify the assumption $\gamma = 0$ introduced in Section 4.1.1 for the limiting case $Pe \to \infty$. In fact, for a fixed value of $\Omega$, one may see from these tables that $\gamma$ approaches continuously 0 when $Pe$ increases and tends to infinity. A similar reasoning holds for the assumption $\gamma = 0$ introduced in Section 4.1.2 for the limiting case $\Omega \to 0$.

Tables 2 and 3 show that $Ra_{cr}$ is a decreasing function of $\Omega$ for a fixed $Pe$ and an increasing function of $Pe$ for a fixed $\Omega$. The former feature can be interpreted physically as the destabilizing effect of the viscous dissipation. This destabilizing effect can be so intense that $Ra_{cr}$ may drop to zero for a sufficiently high value of $\Omega$. Tables 2 and 3 suggest that the critical value of $\Omega$ leading to $Ra_{cr} = 0$ is greater than 55 for $Pe = 5$, 10, 100, and $\infty$, is greater than 40 for $Pe = 2$ and is greater than 25 for $Pe = 1$. For the case $Ra = 0$, precise values of $\Omega_{cr}$, as well as of the corresponding values of $a_{cr}$ and $\gamma_{cr}$, are given in Table 4 for different Péclet numbers. Both $a_{cr}$ and $\Omega_{cr}$ are increasing functions of $Pe$, that attain the asymptotic values given by Eq. (70) when $Pe \to \infty$. Tables 2 and 3 also reveal that the critical wave number, $a_{cr}$, is a monotonic function of $\Omega$ for a fixed $Pe = 10$, 100, $\infty$, but not for $Pe = 1$, 2, 5. More precisely, in the latter case, $a_{cr}$ initially increases with $\Omega$, reaches a maximum and then decreases.

The neutral stability curves for the case $\Omega = 20$ are displayed in Fig. 2 for five different values of $Pe$. Furthermore, the effect of increasing values of $\Omega$ for $Pe = 2$ is illustrated in Fig. 3. Increasing values of $\Omega$ for a fixed Péclet number correspond to an increasing contribution of the frictional heating. Then, Fig. 3 confirms the destabilizing role played by the viscous dissipation.

### 4.2. Longitudinal rolls

The analysis of stability against longitudinal rolls differs from that against transverse rolls for the discrete spectrum of wave numbers,

**Table 2**
Transverse rolls: critical values of $a$, $Ra$ and $\gamma$.

| $\Omega$ | $Pe \to \infty$ | | | $Pe = 100$ | | | $Pe = 10$ | | |
|---|---|---|---|---|---|---|---|---|---|
| | $a_{cr}$ | $Ra_{cr}$ | $\gamma_{cr}$ | $a_{cr}$ | $Ra_{cr}$ | $\gamma_{cr}$ | $a_{cr}$ | $Ra_{cr}$ | $\gamma_{cr}$ |
| 0 | 2.3262 | 27.098 | 0 | 2.3262 | 27.098 | 0 | 2.3262 | 27.098 | 0 |
| $10^{-8}$ | 2.3262 | 27.098 | 0 | 2.3262 | 27.098 | 0.0000 | 2.3262 | 27.098 | 0.0000 |
| $10^{-4}$ | 2.3262 | 27.098 | 0 | 2.3262 | 27.098 | 0.0000 | 2.3262 | 27.098 | 0.0000 |
| 0.001 | 2.3262 | 27.097 | 0 | 2.3262 | 27.097 | 0.0000 | 2.3262 | 27.097 | 0.0000 |
| 0.01 | 2.3262 | 27.093 | 0 | 2.3262 | 27.093 | 0.0000 | 2.3262 | 27.093 | 0.0003 |
| 0.1 | 2.3263 | 27.055 | 0 | 2.3263 | 27.055 | 0.0003 | 2.3263 | 27.055 | 0.0026 |
| 1 | 2.3272 | 26.671 | 0 | 2.3272 | 26.671 | 0.0025 | 2.3272 | 26.671 | 0.0255 |
| 2 | 2.3282 | 26.245 | 0 | 2.3282 | 26.245 | 0.0051 | 2.3282 | 26.244 | 0.0509 |
| 5 | 2.3315 | 24.963 | 0 | 2.3315 | 24.963 | 0.0127 | 2.3312 | 24.957 | 0.1269 |
| 10 | 2.3375 | 22.819 | 0 | 2.3375 | 22.819 | 0.0253 | 2.3365 | 22.797 | 0.2525 |
| 15 | 2.3442 | 20.666 | 0 | 2.3442 | 20.665 | 0.0377 | 2.3420 | 20.617 | 0.3767 |
| 20 | 2.3517 | 18.503 | 0 | 2.3517 | 18.503 | 0.0500 | 2.3477 | 18.416 | 0.4994 |
| 25 | 2.3600 | 16.331 | 0 | 2.3599 | 16.330 | 0.0621 | 2.3537 | 16.196 | 0.6204 |
| 30 | 2.3691 | 14.149 | 0 | 2.3690 | 14.147 | 0.0740 | 2.3599 | 13.955 | 0.7396 |
| 35 | 2.3790 | 11.957 | 0 | 2.3789 | 11.955 | 0.0858 | 2.3665 | 11.695 | 0.8570 |
| 40 | 2.3899 | 9.7554 | 0 | 2.3897 | 9.7520 | 0.0973 | 2.3733 | 9.4149 | 0.9724 |
| 45 | 2.4016 | 7.5430 | 0 | 2.4014 | 7.5387 | 0.1087 | 2.3805 | 7.1153 | 1.0856 |
| 50 | 2.4143 | 5.3199 | 0 | 2.4140 | 5.3147 | 0.1198 | 2.3880 | 4.7962 | 1.1966 |
| 55 | 2.4279 | 3.0860 | 0 | 2.4276 | 3.0798 | 0.1306 | 2.3958 | 2.4576 | 1.3051 |

**Table 3**
Transverse rolls: critical values of $a$, $Ra$ and $\gamma$.

| $\Omega$ | $Pe = 5$ | | | $Pe = 2$ | | | $Pe = 1$ | | |
|---|---|---|---|---|---|---|---|---|---|
| | $a_{cr}$ | $Ra_{cr}$ | $\gamma_{cr}$ | $a_{cr}$ | $Ra_{cr}$ | $\gamma_{cr}$ | $a_{cr}$ | $Ra_{cr}$ | $\gamma_{cr}$ |
| 0 | 2.3262 | 27.098 | 0 | 2.3262 | 27.098 | 0 | 2.3262 | 27.098 | 0 |
| $10^{-8}$ | 2.3262 | 27.098 | 0.0000 | 2.3262 | 27.098 | 0.0000 | 2.3262 | 27.098 | 0.0000 |
| $10^{-4}$ | 2.3262 | 27.098 | 0.0000 | 2.3262 | 27.098 | 0.0000 | 2.3262 | 27.098 | 0.0000 |
| 0.001 | 2.3262 | 27.097 | 0.0001 | 2.3262 | 27.097 | 0.0001 | 2.3262 | 27.097 | 0.0003 |
| 0.01 | 2.3262 | 27.093 | 0.0005 | 2.3262 | 27.093 | 0.0013 | 2.3262 | 27.093 | 0.0026 |
| 0.1 | 2.3263 | 27.055 | 0.0051 | 2.3263 | 27.055 | 0.0128 | 2.3263 | 27.055 | 0.0255 |
| 1 | 2.3272 | 26.671 | 0.0510 | 2.3270 | 26.666 | 0.1274 | 2.3262 | 26.649 | 0.2548 |
| 2 | 2.3281 | 26.241 | 0.1018 | 2.3273 | 26.223 | 0.2546 | 2.3243 | 26.156 | 0.5089 |
| 5 | 2.3305 | 24.941 | 0.2538 | 2.3254 | 24.824 | 0.6341 | 2.3073 | 24.407 | 1.2648 |
| 10 | 2.3335 | 22.731 | 0.5049 | 2.3131 | 22.266 | 1.2586 | 2.2435 | 20.598 | 2.4903 |
| 15 | 2.3353 | 20.468 | 0.7528 | 2.2898 | 19.426 | 1.8705 | 2.1436 | 15.663 | 3.6486 |
| 20 | 2.3358 | 18.153 | 0.9974 | 2.2560 | 16.305 | 2.4670 | 2.0203 | 9.5893 | 4.7112 |
| 25 | 2.3350 | 15.788 | 1.2383 | 2.2130 | 12.906 | 3.0455 | 1.8870 | 2.3618 | 5.6553 |
| 30 | 2.3329 | 13.371 | 1.4753 | 2.1620 | 9.2267 | 3.6033 | – | – | – |
| 35 | 2.3296 | 10.904 | 1.7083 | 2.1045 | 5.2679 | 4.1377 | – | – | – |
| 40 | 2.3250 | 8.3883 | 1.9372 | 2.0422 | 1.0283 | 4.6462 | – | – | – |
| 45 | 2.3192 | 5.8237 | 2.1617 | – | – | – | – | – | – |
| 50 | 2.3122 | 3.2112 | 2.3819 | – | – | – | – | – | – |
| 55 | 2.3040 | 0.55132 | 2.5977 | – | – | – | – | – | – |

$$a = \frac{m\pi}{2s}, \quad m = 1, 2, 3, \ldots \tag{71}$$

This is a consequence of the lateral confinement. However, if we span all the possible aspect ratios $s$, then the wave number $a$ can assume any positive real value. Then, by introducing the dimensionless parameter $\Omega$ defined by Eq. (54) in Eqs. (47)–(49), these equations and the initial conditions discussed in Section 3.2.1 form the initial value problem

$$\Psi_m'' - a^2\Psi_m + aRa\Theta_m = 0, \tag{72}$$

$$\Theta_m'' - a^2\Theta_m + a\left(\frac{\Omega}{Ra}y + 1\right)\Psi_m = 0, \tag{73}$$

$$\Psi_m(0) = 0, \ \Psi_m'(0) = 1, \ \Theta_m(0) = \eta_m, \ \Theta_m'(0) = 0, \tag{74}$$

subject to the constraint equations

$$\Psi_m(1) = 0, \quad \Theta_m(1) = 0. \tag{75}$$

We note that a comparison between Eqs. (59)–(61) and Eqs. (72)–(74) reveals that the two initial value problems are formally coincident. Then, we can infer that, for every assigned $\Omega$, the critical values $a_{cr}(\Omega)$ and $Ra_{cr}(\Omega)$ are those obtained for transverse rolls in the limiting case $Pe \to \infty$ and reported in the first column of Table 2. As a consequence of Eq. (71), for every prescribed value of $\Omega$, there exists a discrete sequence of corresponding critical values of $s$, defined by all the integer multiples of

$$s_{cr}(\Omega) = \frac{\pi}{2a_{cr}(\Omega)}. \tag{76}$$

The value of $s_{cr}$ is a function of $\Omega$, as $a_{cr}(\Omega)$ is the critical wave number obtained for the assigned value of $\Omega$. For a given pair $(s, \Omega)$, the minimum Rayleigh number for neutral stability against longitudinal rolls represents the critical Rayleigh number, $Ra_{cr,L}(s, \Omega)$. We can determine $Ra_{cr,L}(s, \Omega)$ by seeking the minimum over the different integers $m$ of the eigenvalue $Ra$ for the problem Eqs. (72)–(75) with $a$ expressed by Eq. (71). If, for a given $\Omega$, the aspect ratio $s$ is not an integer multiple of $s_{cr}(\Omega)$, then the value of $Ra_{cr,L}(s, \Omega)$ for neutral stability against longitudinal rolls is greater than $Ra_{cr}(\Omega)$. In other words,

$$Ra_{cr,L}(s, \Omega) \geq Ra_{cr}(\Omega), \tag{77}$$

where the equality holds if and only if $s$ is an integer multiple of $s_{cr}(\Omega)$.

**Table 4**
Transverse rolls with $Ra = 0$: critical values of $a$, $\Omega$ and $\gamma$.

| $Pe$ | $a_{cr}$ | $\Omega_{cr}$ | $\gamma_{cr}$ |
|---|---|---|---|
| 0.5 | 1.7437 | 15.085 | 6.5362 |
| 0.75 | 1.7962 | 21.195 | 6.2212 |
| 1 | 1.8472 | 26.480 | 5.9102 |
| 1.5 | 1.9427 | 34.943 | 5.3118 |
| 2 | 2.0271 | 41.165 | 4.7607 |
| 3 | 2.1584 | 49.088 | 3.8384 |
| 4 | 2.2456 | 53.470 | 3.1490 |
| 5 | 2.3022 | 56.026 | 2.6415 |
| 6 | 2.3394 | 57.606 | 2.2624 |
| 7 | 2.3646 | 58.638 | 1.9727 |
| 8 | 2.3822 | 59.343 | 1.7457 |
| 9 | 2.3950 | 59.843 | 1.5640 |
| 10 | 2.4044 | 60.210 | 1.4156 |
| 20 | 2.4367 | 61.438 | 0.7209 |
| 50 | 2.4464 | 61.797 | 0.2899 |
| 100 | 2.4478 | 61.849 | 0.1450 |
| 1000 | 2.4483 | 61.866 | 0.0145 |
| $10^4$ | 2.4483 | 61.867 | 0.0015 |
| $\infty$ | 2.4483 | 61.867 | 0 |

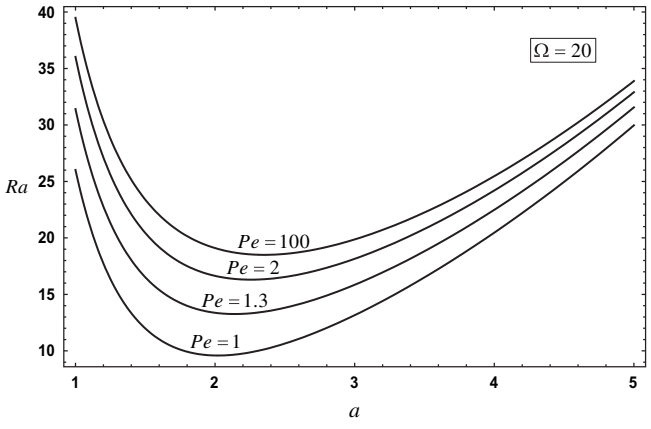


**Fig. 2.** Transverse rolls; neutral stability curves for $\Omega = 20$.

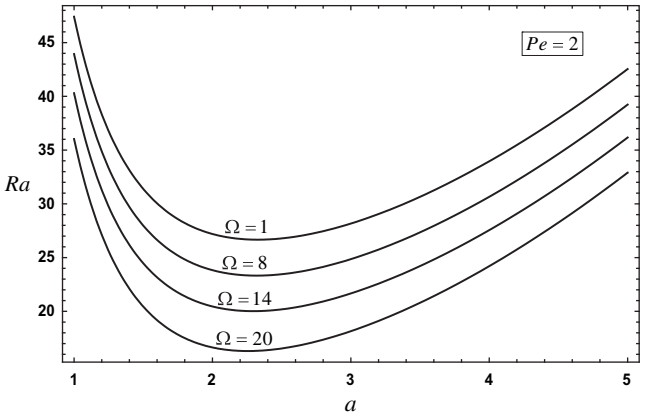


**Fig. 3.** Transverse rolls; neutral stability curves for $Pe = 2$.

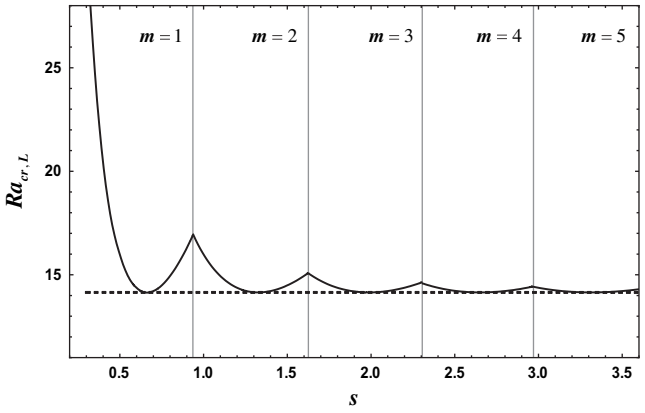


**Fig. 6.** Longitudinal rolls; plot of $Ra_{cr,L}(s, \Omega)$ versus $s$ for $\Omega = 30$, where $s_{cr}(\Omega) = 0.663036$; the dashed line corresponds to $Ra_{cr}(\Omega) = 14.1493$.

As it has been pointed out in Section 4.1.4, for transverse rolls, the critical Rayleigh number is an increasing function of $Pe$ for a fixed $\Omega$. This means that, for a fixed $\Omega$, the highest critical Rayleigh number is obtained in the limit $Pe \to \infty$, *i.e.* the quantity $Ra_{cr}(\Omega)$. From this reasoning and from Eq. (77), one can infer that the preferred mode of instability is transverse rolls. Instability to transverse rolls and instability to longitudinal rolls may become equivalent in the limit $Pe \to \infty$, whenever $s$ coincides with integer multiples of the special critical values defined by Eq. (76). Tables 2 and 3 reveal that instabilities may lead equivalently to the onset of transverse or longitudinal rolls also in the limiting case $\Omega \to 0$ as in this case we loose the dependence on $Pe$. The equivalence between the transverse and the longitudinal rolls is ensured in this limit only if

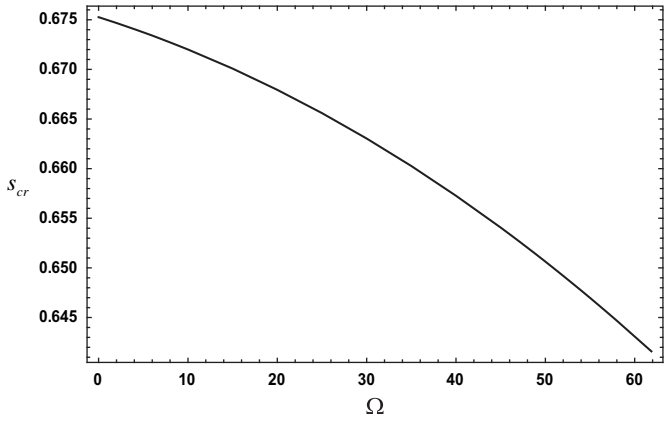


**Fig. 4.** Longitudinal rolls; plot of $s_{cr}$ versus $\Omega$.

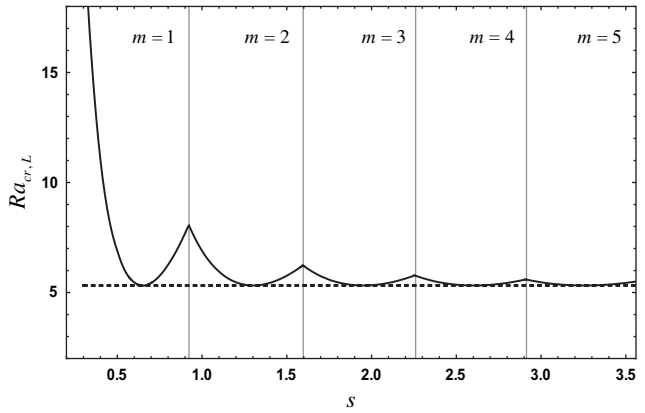


**Fig. 7.** Longitudinal rolls; plot of $Ra_{cr,L}(s, \Omega)$ versus $s$ for $\Omega = 50$, where $s_{cr}(\Omega) = 0.650634$; the dashed line corresponds to $Ra_{cr}(\Omega) = 5.31993$.

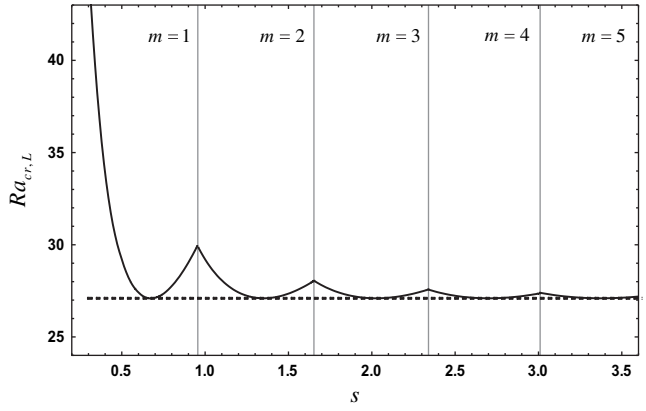


**Fig. 5.** Longitudinal rolls; plot of $Ra_{cr,L}(s, \Omega)$ versus $s$ for $\Omega = 10^{-6}$, where $s_{cr}(\Omega) = 0.675259$; the dashed line corresponds to $Ra_{cr}(\Omega) = 27.0976$.

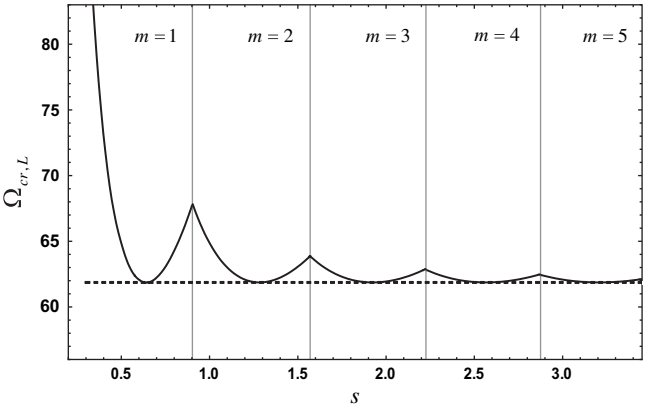


**Fig. 8.** Longitudinal rolls with $Ra = 0$; plot of $\Omega_{cr,L}(s)$ versus $s$; the dashed line corresponds to $\Omega_{cr} = 61.8666$.

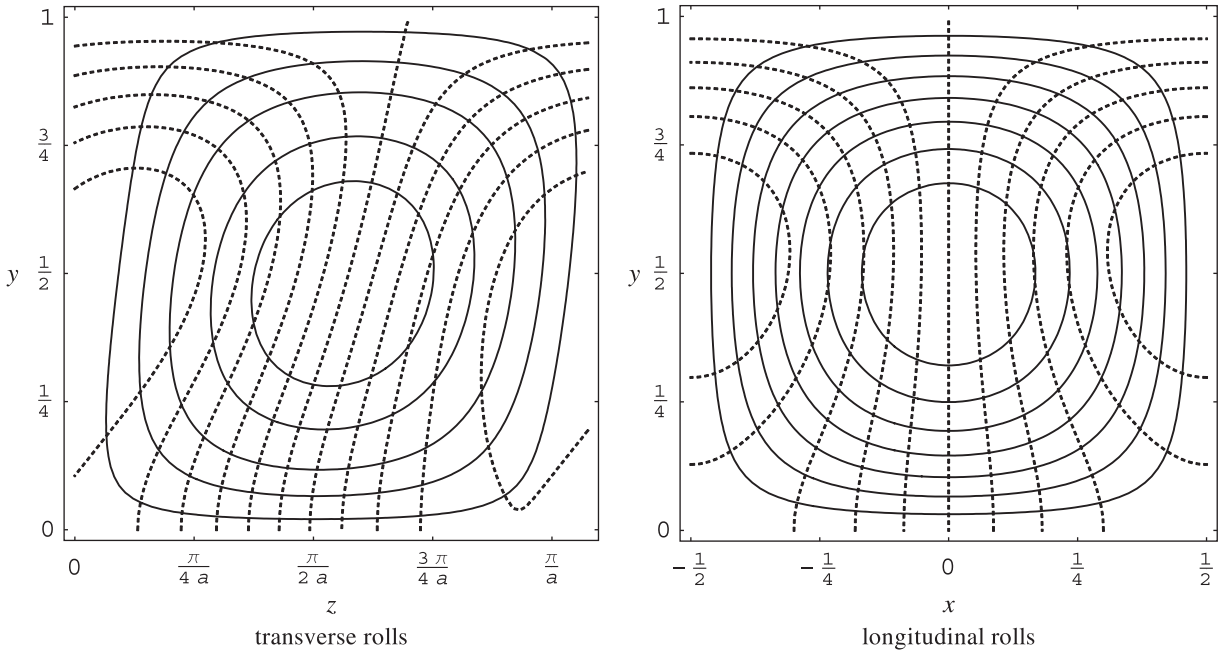


**Fig. 9.** Onset of convection for the case $Ra = 0$ with $Pe = 10$ and $s = 1/2$: streamlines $\psi = constant$ (solid lines) and isotherms $\theta = constant$ (dashed lines) with transverse rolls ($a = 2.40443$, $\Omega = 60.2103$, $t = 0$) and with longitudinal rolls ($a = \pi$, $\Omega = 64.8682$).

$$s = m\,s_{cr}(0) = \frac{m\pi}{2a_{cr}(0)} = 0.675259\,m, \quad m = 1,2,3,\ldots \tag{78}$$

Fig. 4 displays the plot of $s_{cr}(\Omega)$. We mention that this function is defined, on account of Eq. (70), in the interval $0 < \Omega \leq \Omega_{cr}$. In fact, outside this interval, the flow system becomes unstable even with a vanishing heat flux at the bottom boundary. Fig. 4 shows that $s_{cr}(\Omega)$ is a monotonic weakly-decreasing function of $\Omega$.

Figs. 5–7 illustrate the behaviour of $Ra_{cr,L}(s, \Omega)$ versus $s$ for three different values of $\Omega$: $10^{-6}$, 30 and 50. There is a common qualitative feature of these three figures. The plots display a sequence of local minima where $s$ is an integer multiple of $s_{cr}(\Omega)$ and, as a consequence of Eq. (77), $Ra_{cr,L}(s, \Omega) = Ra_{cr}(\Omega)$. As $s$ increases, different $m$-modes yield the lowest critical Rayleigh number. A transition from each $m$-mode to the $(m + 1)$-mode occurs in Figs. 5–7 at the cusp points.

The critical values of the Rayleigh number for the onset of longitudinal rolls define the function $Ra_{cr,L}(s, \Omega)$. For a given $s$, $Ra_{cr,L}(s, \Omega)$ is a monotonic decreasing function of $\Omega$ such that, for a certain threshold value $\Omega = \Omega_{cr,L}(s)$, the critical Rayleigh number becomes zero. A similar feature has been described for transverse rolls in Section 4.1.3. Then, $\Omega = \Omega_{cr,L}(s)$ is the root of the algebraic equation

$$Ra_{cr,L}(s, \Omega) = 0. \tag{79}$$

As a consequence of Eqs. (70) and (76), $\Omega_{cr,L}(s) \geq 61.8666$, where the equality holds only if $s$ is an integer multiple of $s_{cr} = 0.641595$. Fig. 8 illustrates the behaviour of function $\Omega_{cr,L}(s)$. One can easily conclude that the qualitative form of the plot is rather similar to Figs. 5–7, with the same interpretation of the cusp points. Fig. 8 provides a description of the critical conditions for the onset of longitudinal rolls when the heat flux at the bottom boundary becomes zero, namely when $Ra \to 0$.

Fig. 9 displays the streamlines $\psi = constant$ and the isotherms $\theta = constant$ at the onset of either transverse roll or longitudinal roll instability, for the sample case $Ra = 0$, $Pe = 10$ and $s = 1/2$. This sample case is one where the convective instability is activated only by the action of the viscous dissipation effect, since no heat flux is supplied at the bottom boundary ($Ra = 0$). For this case, instability to transverse rolls occurs when $a = 2.40443$ and $\Omega = 60.2103$. Transverse rolls travel in the $z$-direction ($\lambda_2 \neq 0$), so that the left frame of Fig. 9 is referred to $t = 0$. On the other hand, longitudinal rolls at neutral stability conditions, $a = \pi$ and $\Omega = 64.8682$, are time-independent. Fig. 9 illustrates the qualitative features of the convection cells for transverse and longitudinal rolls. The main difference between the two cells is the evident bending of the transverse roll in the streamwise direction.

## 5. Conclusions

The onset of convective roll instabilities has been investigated for a horizontal porous channel bounded by an isoflux bottom wall, a top isothermal wall and two vertical adiabatic boundaries. A basic horizontal flow has been assumed and the effect of viscous dissipation has been taken into account. The most significant results obtained are resumed below.

1. The governing parameters are the Gebhart number, the Péclet number and the Rayleigh number, as well as the aspect ratio of the rectangular cross-section. A vanishingly small Gebhart number yields the limiting case of no viscous dissipation, while a vanishingly small Rayleigh number corresponds to an adiabatic bottom boundary.
2. If, for a given Péclet number, the Gebhart number increases, then the critical Rayleigh number for the onset of transverse rolls decreases and eventually becomes zero, for a sufficiently high Gebhart number. In this regime, the thermoconvective instabilities are purely induced by the contribution of the internal viscous heating.
3. The preferred mode of instability is transverse rolls. The critical Rayleigh number for the onset of longitudinal rolls is generally higher than that for transverse rolls and depends on the aspect ratio of the rectangular cross-section. In the limiting case of

a very large Péclet number and for special values of the channel aspect ratio, the critical values of the Rayleigh number against transverse and longitudinal rolls may be coincident.

This special flow problem is one of the many that may be of interest either for engineering or for geophysics and astrophysics. In fact, the basic feature of the heating from below and the concurrent effect of the frictional heating associated with the basic flow characterise this problem as an instance of a wide class of similar problems. We mention that other possible assignments of the thermal boundary conditions may be considered leading to a heating from below. One can assume an isothermal bottom boundary with a temperature higher than the top boundary, or one can assume a convective heating of the bottom surface through a boundary condition of the third kind. Thus, the subject of thermoconvective instabilities with viscous dissipation in fluid saturated porous media offers interesting opportunities for future research.

## References

[1] C.W. Horton, F.T. Rogers Jr., Convection currents in a porous medium. J. Appl. Phys. 16 (1945) 367–370.
[2] E.R. Lapwood, Convection of a fluid in a porous medium. Proc. Camb. Philos. Soc. 44 (1948) 508–521.
[3] M. Prats, The effect of horizontal fluid flow on thermally induced convection currents in porous mediums. J. Geophys. Res. 71 (1966) 4835–4838.
[4] D.A. Nield, A. Bejan, Convection in Porous Media, third ed. Springer, New York, 2006.
[5] D.A.S. Rees, The stability of Darcy–Bénard convection. in: K. Vafai (Ed.), Handbook of Porous Media. Marcel Dekker, 2000, pp. 521–558.
[6] P.A. Tyvand, Onset of Rayleigh–Bénard convection in porous bodies. in: D. B. Ingham, I. Pop (Eds.), Transport Phenomena in Porous Media II. Elsevier, 2002, pp. 82–112.
[7] A. Nakayama, I. Pop, Free convection over a non-isothermal body in a porous medium with viscous dissipation. Int. Comm. Heat Mass Transf. 16 (1989) 173–180.
[8] P.V.S.N. Murthy, Thermal dispersion and viscous dissipation effects on non-Darcy mixed convection in a fluid saturated porous medium. Heat Mass Transf. 33 (1998) 295–300.
[9] D.A. Nield, Resolution of a paradox involving viscous dissipation and nonlinear drag in a porous medium. Transp. Porous Media 41 (2000) 349–357.
[10] D.A.S. Rees, E. Magyari, B. Keller, The development of the asymptotic viscous dissipation profile in a vertical free convective boundary layer flow in a porous medium. Transp. Porous Media 53 (2003) 347–355.
[11] D.A.S. Rees, E. Magyari, B. Keller, Vortex instability of the asymptotic dissipation profile in a porous medium. Transp. Porous Media 61 (2005) 1–14.
[12] W.P. Breugem, D.A.S. Rees, A derivation of the volume-averaged Boussinesq equations for flow in porous media with viscous dissipation. Transp. Porous Media 63 (2006) 1–12.
[13] D.A. Nield, The modeling of viscous dissipation in a saturated porous medium. ASME J. Heat Transf. 129 (2007) 1459–1463.
[14] A. Barletta, M. Celli, D.A.S. Rees, The onset of convection in a porous layer induced by viscous dissipation: a linear stability analysis. Int. J. Heat Mass Transf. 52 (2009) 337–344.
[15] A. Barletta, D.A.S. Rees, Stability analysis of dual adiabatic flows in a horizontal porous layer. Int. J. Heat Mass Transf. 52 (2009) 2300–2310.
[16] L. Storesletten, A. Barletta, Linear instability of mixed convection of cold water in a porous layer induced by viscous dissipation. Int. J. Thermal Sci. 48 (2009) 655–664.
[17] A. Barletta, M. Celli, D.A.S. Rees, Darcy–Forchheimer flow with viscous dissipation in a horizontal porous layer: onset of convective instabilities. ASME J. Heat Transf. 131 (2009) 072602.
[18] D.A. Nield, A. Barletta, Extended Oberbeck–Boussinesq approximation study of convective instabilities in a porous layer with horizontal flow and bottom heating, Int. J. Heat Mass Transf., in press.
[19] A. Barletta, E. Rossi di Schio, L. Storesletten, Convective roll instabilities of throughflow with viscous dissipation in a horizontal porous layer, Transp. Porous Media, in press, DOI 10.1007/s11242-009-9417-y.
[20] G.M. Homsy, A.E. Sherwood, Convective instabilities in porous media with through flow. AIChE J. 22 (1976) 168–174.